

## Dynamical response of the Hodgkin-Huxley model in the high-input regime

Stefano Luccioli,<sup>1,2,\*</sup> Thomas Kreuz,<sup>1,†</sup> and Alessandro Torcini<sup>1,3,‡</sup>

<sup>1</sup>*Istituto dei Sistemi Complessi, Consiglio Nazionale delle Ricerche, via Madonna del Piano 10, I-50019 Sesto Fiorentino, Italy*

<sup>2</sup>*Istituto Nazionale di Fisica Nucleare, Sezione di Firenze, via Sansone, 1 - I-50019 Sesto Fiorentino, Italy*

<sup>3</sup>*Centro Interdipartimentale per lo Studio delle Dinamiche Complesse, via Sansone, 1 - I-50019 Sesto Fiorentino, Italy*

(Received 15 December 2005; published 6 April 2006)

The response of the Hodgkin-Huxley neuronal model subjected to stochastic uncorrelated spike trains originating from a large number of inhibitory and excitatory post-synaptic potentials is analyzed in detail. The model is examined in its three fundamental dynamical regimes: silence, bistability, and repetitive firing. Its response is characterized in terms of statistical indicators (interspike-interval distributions and their first moments) as well as of dynamical indicators (autocorrelation functions and conditional entropies). In the silent regime, the coexistence of two different coherence resonances is revealed: one occurs at quite low noise and is related to the stimulation of subthreshold oscillations around the rest state; the second one (at intermediate noise variance) is associated with the regularization of the sequence of spikes emitted by the neuron. Bistability in the low noise limit can be interpreted in terms of jumping processes across barriers activated by stochastic fluctuations. In the repetitive firing regime a maximization of incoherence is observed at finite noise variance. Finally, the mechanisms responsible for the different features appearing in the interspike-interval distributions (like multimodality and exponential tails) are clearly identified in the various regimes.

DOI: [10.1103/PhysRevE.73.041902](https://doi.org/10.1103/PhysRevE.73.041902)

PACS number(s): 87.10.+e, 05.45.-a, 87.17.Aa, 05.40.Ca

### I. INTRODUCTION

Neuronal models represent a fundamental benchmark to investigate the dynamical response of excitable systems under the influence of noise. One of the main reasons justifying the interest of neuroscientists for this subject resides in the observation that *in vivo* neocortical neurons are subjected to a constant bombardment of inhibitory and excitatory post-synaptic potentials (EPSPs and IPSPs), somehow resembling a background noise. As a consequence in the last decades a large number of numerical and theoretical studies have been devoted to the characterization of the response of simple and more elaborate neuronal models under the influence of a large variety of stochastic inputs [1–3].

Among the many proposed biophysical models the one introduced by Hodgkin and Huxley in 1952 [4] can still be considered as a valid framework for exploring neural excitability, due to its relative simplicity combined with the fact that it embodies the major features of membrane potential evolution [5]. In particular, in order to understand the origin of the variability observed in the distribution of spikes emitted by cortical neurons [6] the response of the Hodgkin-Huxley (HH) model has recently been studied under the influence of additive noise [7,8] or subjected to trains of post-synaptic potentials [7,9,10].

*Stochastic resonance* (SR) [11] and *coherence resonance* (CR) [12,13] represent some of the most interesting phenomena observed experimentally and numerically for excitable neuronal systems driven by noise. While SR is related to the enhanced ability of neurons to detect weak (periodic or aperiodic) signals when subjected to additive noise, CR refers to the regularization of the response of the system at an optimal noise intensity in the absence of an external signal (for a comprehensive review see Ref. [14]). For neuronal systems evidence of CR have been reported experimentally for the cat's spinal and cortical neural ensembles [15] and theoretically for the following models: FitzHugh-Nagumo [13], leaky integrate-and-fire [16,17], Hindmarsh-Rose [18], and Morris-Lecar [19]. CR has also been observed for the HH model [20,21], but these results mainly refer to additive continuous noise and to the silent regime near the saddle-node bifurcation of limit cycles.

Our aim is to perform a detailed analysis of the response of the HH model subjected to many stochastic trains of EPSPs and IPSPs in its three fundamental dynamical regimes: the silent, the bistable, and the repetitive firing ones. The neuron is studied in the so-called *high-input regime* [6], i.e., when it receives hundreds or thousands of post-synaptic inputs per emitted spike. In this situation the stochastic input can simply be characterized in terms of its average, representing the bifurcation parameter of the model, and its variance. Most of the attention is devoted to the mechanisms responsible for neuronal firing in the different dynamical regimes and to the characterization of CR in terms of dynamical and statistical indicators. In particular, we show that the conditional entropies can be employed as powerful indicators to detect coherence, similar to what has previously been done to characterize stochastic resonance for a Schmitt trigger [22]. Sound evidence of two coexisting CRs are reported, the first one related to subthreshold oscillations occurring at very low noise fluctuations in the absence of spiking and the second one due to the regularization of the emitted spike trains. In the regime of bistability the intermittent dynamics between the two stable dynamical states is interpreted in terms of jumping processes across activation barriers induced by noise fluctuations. Finally, evidence of incoherence

riodic) signals when subjected to additive noise, CR refers to the regularization of the response of the system at an optimal noise intensity in the absence of an external signal (for a comprehensive review see Ref. [14]). For neuronal systems evidence of CR have been reported experimentally for the cat's spinal and cortical neural ensembles [15] and theoretically for the following models: FitzHugh-Nagumo [13], leaky integrate-and-fire [16,17], Hindmarsh-Rose [18], and Morris-Lecar [19]. CR has also been observed for the HH model [20,21], but these results mainly refer to additive continuous noise and to the silent regime near the saddle-node bifurcation of limit cycles.

\*Electronic address: [luccioli@inoa.it](mailto:luccioli@inoa.it)

†Electronic address: [kreuz@inoa.it](mailto:kreuz@inoa.it)

‡Electronic address: [alessandro.torcini@isc.cnr.it](mailto:alessandro.torcini@isc.cnr.it)

TABLE I.  $\alpha_X(V)$  and  $\beta_X(V)$  functions ( $X=m,n,h$ ) entering in Eq. (2) for the voltage expressed in mV.

$X$	$\alpha_X(V)(s^{-1})$	$\beta_X(V)(s^{-1})$
$m$	$0.1(V+40)/(1-\exp[-(V+40)/10])$	$4\exp[-(V+65)/18]$
$n$	$0.01(V+55)/(1-\exp[-(V+55)/10])$	$0.125\exp[-(V+65)/80]$
$h$	$0.07\exp[-(V+65)/20]$	$1/(\exp[-(V+35)/10]+1)$

maximization in the repetitive firing regime is presented.

The model and the various employed indicators, namely the distribution of the interspike-interval (ISI), the spike-triggered averages, the autocorrelation function of the signal, and of the ISIs, and the conditional entropies are introduced in Sec. II. The results for the silent regime are reported in Sec. III, while the bistable and repetitive firing regimes are examined in Secs. IV and V, respectively. Sec. VI contains a summary of the results and concluding remarks.

## II. MODELS AND TOOLS

### A. The Hodgkin-Huxley model

The Hodgkin-Huxley (HH) model describes the dynamical evolution of the membrane potential  $V(t)$  and it can be written as

$$-C\frac{dV}{dt} = g_{Na}m^3h(V - E_{Na}) + g_Kn^4(V - E_K) + g_L(V - E_L) - I(t), \quad (1)$$

where  $I(t)$  is an external current and the evolution of the gating variables  $X=m,n,h$  is ruled by three ordinary differential equations (ODE's) of the form

$$\frac{dX}{dt} = \alpha_X(V)(1 - X) - \beta_X(V)X. \quad (2)$$

The parameters entered in Eq. (1) are  $C=1\mu\text{F}/\text{cm}^2$ ,  $E_{Na}=50\text{ mV}$ ,  $E_K=-77\text{ mV}$ ,  $E_L=-54.4\text{ mV}$ ,  $g_{Na}=120\text{ mS}/\text{cm}^2$ ,  $g_K=36\text{ mS}/\text{cm}^2$ , and  $g_L=0.3\text{ mS}/\text{cm}^2$ . The expressions of the nonlinear functions  $\alpha_X(V)$  and  $\beta_X(V)$  are explicitly reported in Table I. An estimation of an effective ‘‘passive’’ membrane time constant for the HH model is reported in Ref. [2] and this amounts to  $\approx 1\text{ ms}$ .

We consider the single HH model subjected to  $N_E$  (respectively  $N_I$ ) uncorrelated trains of excitatory (respectively inhibitory) post-synaptic potentials (EPSPs, respectively IPSPs). Each post-synaptic potential (PSP) is schematized as an instantaneous variation of the membrane potential by a positive (respectively negative) amount  $\Delta V$  for excitatory (respectively inhibitory) synapses. Similarly to what has been done in Ref. [9], the amplitude of each voltage kick is assumed to be  $0.5\text{ mV}$ , i.e., reasonably small ( $\approx 7\%$ ) with respect to the distance between the ‘‘threshold’’ for spike initiation for rapid EPSPs and the resting potential ( $\approx 6-7\text{ mV}$ ) [1,23]. Moreover, amplitudes  $\approx 0.5\text{ mV}$  are comparable with average EPSPs experimentally measured for pyramidal neurons in the visual cortex of rats [2]. This amounts to exciting the neuron ((1),(2)) with an impulsive current

$$I(t) = Q \left[ \sum_{k=1}^{N_e} \sum_l \delta(t - t_k^l) - \sum_{m=1}^{N_i} \sum_n \delta(t - t_m^n) \right] \quad (3)$$

where  $t_k^l$  (respectively  $t_m^n$ ) are the arrival times of the excitatory (respectively inhibitory) PSPs and  $Q=C\Delta V$  is the charge associated to each kick. The dynamics has been integrated by employing a fourth order Runge-Kutta scheme with a time step of  $\delta t=10^{-5}-10^{-2}\text{ ms}$ . A spike is identified when  $V(t)$  overcomes a fixed detection threshold  $\Theta=-5\text{ mV}$ . The results reported in this paper refer to averages performed over time spans corresponding to 30 000 to 600 000 emitted spikes or (in the low noise limit, where spikes are more rare) at least to an integration time of  $t \approx 1000-10\,000\text{ s}$ .

In order to reproduce realistic inputs received by cortical neurons, for each afferent synapse the time interval distribution between PSP inputs is chosen Poissonian with an average frequency  $\nu_0=100\text{ Hz}$  [6]. Since the trains coming from different neurons are assumed to be uncorrelated, this amounts to considering only two Poissonian distributed input trains of kicks of amplitude  $\Delta V$ , one for the excitatory and one for the inhibitory neurons with frequencies  $\nu_E=N_e \times \nu_0$  and  $\nu_I=N_I \times \nu_0$ , respectively. We consider a number of input neurons of the order of  $\sim 100-1000$ , thus the HH neuron is stimulated with average frequencies  $\nu_E(\nu_I) \sim 10^4-10^5\text{ Hz}$ , consistent with a high-input regime [6].

The stochastic input can be characterized in terms of the net spike count within a temporal window  $\Delta T$

$$N(\Delta T) = \sum_{k=1}^{N_e} n_k^E(\Delta T) - \sum_{m=1}^{N_i} n_m^I(\Delta T) \quad (4)$$

where  $n_k^E(\Delta T)$  [respectively  $n_m^I(\Delta T)$ ] represents the number of afferent EPSPs (respectively IPSPs) received from neuron  $k$  (respectively  $m$ ) in the interval  $\Delta T$ . According to the theory of renewal processes [1] each variable  $n(\Delta T)$  has a Gaussian distribution with average  $\langle n(\Delta T) \rangle = \Delta T/a_{ISI}$  and variance  $\langle n^2(\Delta T) \rangle - \langle n(\Delta T) \rangle^2 = (\Delta T v_{ISI})/a_{ISI}^3$ , where  $a_{ISI}$  and  $v_{ISI}$  indicate average and variance of the ISI distribution. In particular for Poissonian distributed ISIs with an average frequency of  $\nu_0$ :  $a_{ISI}=1/\nu_0$  and  $v_{ISI}=1/\nu_0^2$ .

By assuming statistically independent input trains, also  $N[\Delta(T)]$  follows a Gaussian distribution with an average and variance given by

$$\langle N(\Delta T) \rangle = (N_e - N_i) \frac{\Delta T}{a_{ISI}},$$

$$\text{Var}[N(\Delta T)] = (N_e + N_i) \frac{(\Delta T v_{ISI})}{a_{ISI}^3} = \sigma^2 \frac{\Delta T}{a_{ISI}}. \quad (5)$$

Here it has also been assumed that the excitatory and inhibitory inputs are characterized by the same  $a_{ISI}$  and  $v_{ISI}$ . The parameter  $\sigma = (\sqrt{(N_e + N_i)v_{ISI}})/a_{ISI}$  measures the standard deviation of the stochastic input process.

In the high-input regime the distribution of  $N[\Delta(T)]$  turns out to be the same for input ISIs following a Poissonian or a uniform distribution

$$P_U(t) = \begin{cases} \frac{\nu_0}{2\varepsilon} & \text{if } \frac{(1-\varepsilon)}{\nu_0} \leq t \leq \frac{(1+\varepsilon)}{\nu_0}, \\ 0 & \text{otherwise,} \end{cases} \quad (6)$$

provided that both distributions have the same average and variance. For  $P_U(t)$ , with  $0 \leq \varepsilon \leq 1$ ,  $a_{ISI} = 1/\nu_0$ ,  $v_{ISI} = \varepsilon^2/(\nu_0^2 3)$ , and  $\sigma = \varepsilon \sqrt{(N_e + N_i)}/3$ . Since we are interested in analyzing the effect of the variance of the stochastic process on the response of the HH model for fixed  $\langle N(\Delta T) \rangle$ , we will consider uniformly distributed ISIs, because this kind of distribution allows one to reach extremely small values of the variance (by lowering the  $\varepsilon$ -parameter) without modifying the average.

Both for Poissonian and uniform distributions with fixed  $a_{ISI} = 1/\nu_0$  the average current stimulating the neuron is given by

$$\bar{I} = \frac{C\Delta V \langle N(\Delta T) \rangle}{\Delta T} = C\Delta V \nu_0 (N_e - N_i). \quad (7)$$

The bifurcation parameter  $\bar{I}$  determines in which dynamical regime the neuron is operating.

Since it is equivalent to stimulate a neuron with a constant current  $I(t) \equiv I_{dc}$  or with a periodic train of kicks of sufficiently high frequency  $\bar{\nu}$ , the frequency-current response curve (usually obtained with a constant input current) can also be recovered by considering a periodic input originating from  $N_i$  inhibitory and  $N_e$  excitatory synapses each firing with a frequency  $\nu_0$  (cf. Fig. 1).

Three principal dynamical regimes can be singled out for the HH model subject to a constant current stimulation [24]. For small currents the HH model is in a silent regime, i.e., its dynamics is always attracted by a stable fixed point. In particular, the relaxation towards this state is characterized by damped oscillations, since it is a focus. By increasing the current the fixed point loses its stability via a sub-critical Hopf bifurcation for  $\bar{I} = I_{HB} \approx 9.78 \mu\text{A}/\text{cm}^2$ . The unstable limit cycles emerging at  $I_{HB}$  annihilates via a saddle-node bifurcation with stable periodic oscillations, corresponding to tonic firing, at a lower value of the current  $\bar{I} = I_{SN} \approx 6.27 \mu\text{A}/\text{cm}^2$ . Therefore the following three dynamical regimes can be identified:

1. A silent regime for  $\bar{I} < I_{SN}$ ;
2. A bistable regime, where the fixed point coexists with a stable limit cycle solution for  $I_{SN} < \bar{I} < I_{HB}$ ;
3. A periodic firing regime for  $\bar{I} > I_{HB}$ .

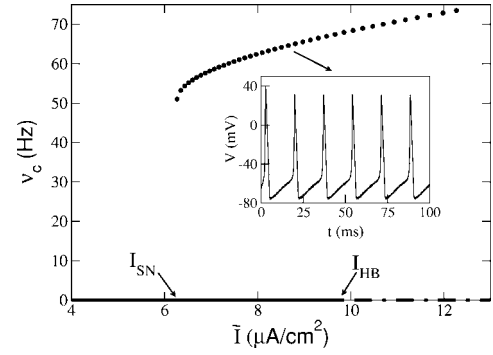


FIG. 1. The filled circles represent the frequency-current response curve ( $\nu_c$  versus  $\bar{I}$ ) obtained by considering a periodic train of kicks of amplitude  $\Delta V = 0.5$  mV and frequency  $\bar{\nu} = \bar{I}/(C\Delta V) = \nu_0(N_e - N_i)$ . The solid (respectively dash-dotted) line indicates the stable (respectively unstable) fixed point solution. In the inset the time evolution of the membrane potential  $V(t)$ , corresponding to a typical limit cycle solution, is shown.

## B. Statistical and dynamical indicators

In order to characterize the output of the neuron and to examine the coherence effects in the response we have employed the following indicators:

(i) The distribution of the output interspike intervals  $P_{ISI}(t)$  and its first moments: the average ISI ( $A_{ISI}$ ) and the corresponding standard deviation ( $S_{ISI}$ );

(ii) The spike-triggered average potential (STAP) [25] that gives the average shape of the membrane potential preceding the emission of a spike and the spike-triggered average input fluctuations (STAF):

$$q(t) = \frac{[N_i(\Delta T) - \langle N(\Delta T) \rangle]}{\sqrt{\text{Var}[N(\Delta T)]}}, \quad (8)$$

where  $N_i(\Delta T)$  is the net spike count at time  $t < 0$  before a spike emission occurring at  $t = 0$ , while the expressions of  $\langle N(\Delta T) \rangle$  and  $\text{Var}[N(\Delta T)]$  are reported in Eqs. (5). The STAF (8) can be related to current fluctuations, estimated over a time window  $\Delta T$ , with respect to their average value  $\bar{I}$  [see Eq. (7)]. A positive (respectively negative) value of  $q$  at a certain time  $t < 0$  indicates a correlation between a positive (respectively negative) current fluctuation at that time and the emission of a spike at  $t = 0$ .

(iii) The coefficient of variation of the ISIs

$$R = \frac{S_{ISI}}{A_{ISI}}, \quad (9)$$

typically employed to characterize the nature of a process, being  $R = 0$  for a perfectly periodic response and  $R = 1$  for Poissonian output;

(iv) The normalized autocorrelation function  $C(t)$  for the membrane potential and the correlation time [13] defined as

$$\tau_c = \int_0^\infty C^2(t) dt. \quad (10)$$

As a further indicator we have employed the *conditional entropies*  $h(N)$  [26]. In order to define these quantities, we need to digitize the output of the neuron in a binary sequence, where 1 and 0 indicates, respectively presence or absence of a spike in a certain time window  $\Delta t$ . The choice of the resolution  $\Delta t$  employed to analyze the output is crucial [27]<sup>1</sup>.

Indicating with  $s_k$  the binary symbol associated to the  $k$ th window of the time series and with  $W_N=(s_{i+1}, s_{i+2}, \dots, s_{i+N})$  a sequence of symbols (word) of length  $N$ , the probability that a certain word will be observed is  $P(W_N)$ . The Shannon block entropy is then defined as

$$H(N) = - \sum_{\{W_N\}} P(W_N) \log_2 P(W_N) \quad (11)$$

where the sum is extended to all the  $2^N$  possible words of length  $N$ . The conditional entropies are given by the following difference [27]:

$$h(N) = H(N+1) - H(N) = - \left\langle \sum_{\{s_{N+1}\}} P(s_{N+1}|W_N) \log_2 P(s_{N+1}|W_N) \right\rangle_{\{W_N\}}, \quad (12)$$

where the brackets indicate the average over all possible sequences of length  $N$  preceding the symbol  $s_{N+1}$  and  $P(s_{N+1}|W_N)$  is the conditional probability to observe the symbol  $s_{N+1}$  once the word  $W_N$  has been registered. By definition we set  $h(0)=H(1)$ .

The conditional entropies represent the average information gained by the knowledge of the  $(N+1)$ -th symbol of a time series, once the other  $N$  symbols are already known. For sufficiently long words, if the examined process can be considered as “ergodic,”  $h(N)$  tends to an asymptotic value  $h_A$ , the length  $M$  for which the saturation is attained gives the order (the memory) of the Markovian process able to reproduce the considered dynamics [28]. For a regular process (e.g., a periodic state)  $h_A=0$ , while for a purely stochastic process the conditional entropies attain their maximal value, i.e.,  $h_A=1$  (bit)<sup>2</sup>.

As already mentioned, the conditional entropies have been successfully employed to characterize SR [22]. In par-

<sup>1</sup>The time window  $\Delta t$  should be chosen in an appropriate way to avoid on one side observation of two spikes within the same window and on the other side to have extremely long series of zeros, that would spoil the statistical analysis. A good choice of  $\Delta t$  is the refractory period of the neuron following the emission of a spike and an upper bound for this time can be given by the measured minimal ISI value. Since the period of relative refractoriness decreases upon increasing the amount of noise, for each current we have chosen  $\Delta t$  to be the minimal ISI measured for the maximum noise variance considered. As a matter of fact  $\Delta t=5$  ms has been used for all current values, apart from  $\bar{I}=0$ , where  $\Delta t=7$  ms was more appropriate.

<sup>2</sup>From a numerical point of view it is known that the estimation of Shannon entropy (11) from finite samples can lead to underestimation of  $H(N)$ . In order to reduce the systematic errors arising from naive estimations of  $P(W_N)$  we have employed the analytic estimator recently introduced by Grassberger [29].

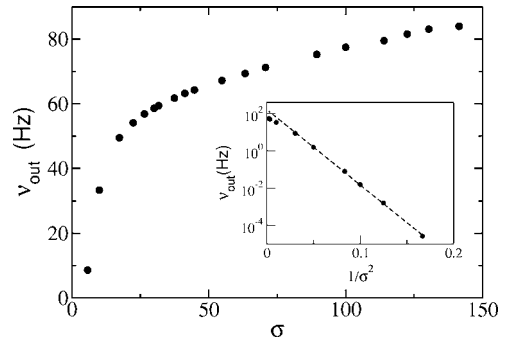


FIG. 2. Average firing rate  $v_{out}$  as a function of  $\sigma$  for  $\bar{I}=5 \mu\text{A}/\text{cm}^2$ . In the inset the frequency is plotted in a lin-log scale as a function of  $1/\sigma^2$  for  $\sigma^2 < 500$ . The dashed line is an exponential fit  $y=A \times \exp[-\sigma_c^2/\sigma^2]$  in the range  $6 < \sigma^2 < 20$  with  $A=162$  and  $\sigma_c^2 \approx 93$ .

ticular a clear minimum for  $h_A$  was observed in correspondence to an optimal noise amplitude giving rise to a maximum in the signal-to-noise ratio (SNR), that is a typical signature of SR. The minimum in  $h_A$  was associated with the most ordered (coherent) structure of the output binary sequence.

Finally, in order to characterize the correlations present in the binary sequence we use the following autocorrelation function [2]:

$$C_{bin}(k) = \frac{\sum_i (\langle s_i s_{i+k} \rangle - \langle s_i \rangle \langle s_{i+k} \rangle)}{\sum_i (\langle s_i^2 \rangle - \langle s_i \rangle^2)} \quad (13)$$

and the associated correlation time  $\tau_{bin}$  defined as in Eq. (10).

In the next sections we investigate the response of the HH model stimulated by stochastic spike trains in the three dynamical regimes shown in Fig. 1.

### III. SILENT REGIME

In the regime where the neuron subjected to a constant current does not fire, i.e., in the range  $\bar{I} < I_{SN} \approx 6.27 \mu\text{A}/\text{cm}^2$ , the presence of noise in the input (characterized by the standard deviation of the noise  $\sigma$ ) induces stochastic firing of the model with an average firing rate  $v_{out} \equiv 1/I_{ISI}$  steadily increasing with  $\sigma$  (as shown in Fig. 2 for  $\bar{I}=5 \mu\text{A}/\text{cm}^2$ ).

For a fixed average input current  $\bar{I}$  the ISI-distribution depends strongly on the standard deviation  $\sigma$  of the noise (cf. Fig. 3). For low noise  $P_{ISI}(t)$  exhibits a multimodal structure with an exponential tail, for increasing noise the additional peaks and the tail disappear gradually. In the high noise limit  $P_{ISI}(t)$  tends to an inverse Gaussian [1,30].

In the following Sec. III A we discuss the mechanisms responsible for the firing activity of the neuron in the low and high noise limits, while Sec. III B is devoted to coherence resonance phenomena observed for the intermediate level of noise fluctuations.

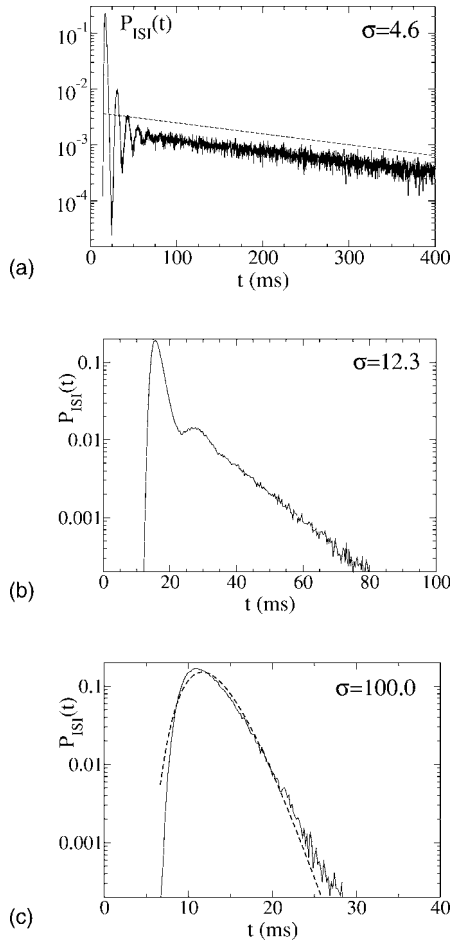


FIG. 3. Probability density distribution  $P_{ISI}(t)$  for  $\bar{I} = 6.15 \mu\text{A}/\text{cm}^2$ . The figures refer to three different values of  $\sigma$ : (a) 4.6, (b) 12.3, and (c) 100.0. The dashed line in (a) indicates the slope of the exponential tail, while in (c) it represents an inverse Gaussian distribution with the same average and the same variance as the original  $P_{ISI}(t)$ .

#### A. Response of the neuron to low and high noise

Let us discuss the origin of the main features present in  $P_{ISI}(t)$  at low noise. The coexistence of multipicks and the exponential tail in Fig. 3(a) suggests that at least two different mechanisms are responsible for the firing of the neuron.

##### 1. Spikes triggered by relaxation oscillations

We can safely affirm that the multiple peaks in the  $P_{ISI}(t)$  are associated with the relaxation oscillations of the membrane potential towards the rest state following the emission of a spike. However, a linear stability analysis around the stable fixed point can provide the oscillation periods around the focus, but is not sufficient to fully characterize the relaxation dynamics, that also exhibits nonlinear aspects.

In order to understand if these oscillations are responsible for the multimodal structure of  $P_{ISI}(t)$ , we have stimulated the model ((1), (2)) with a step current of amplitude  $\bar{I}$ , i.e.,

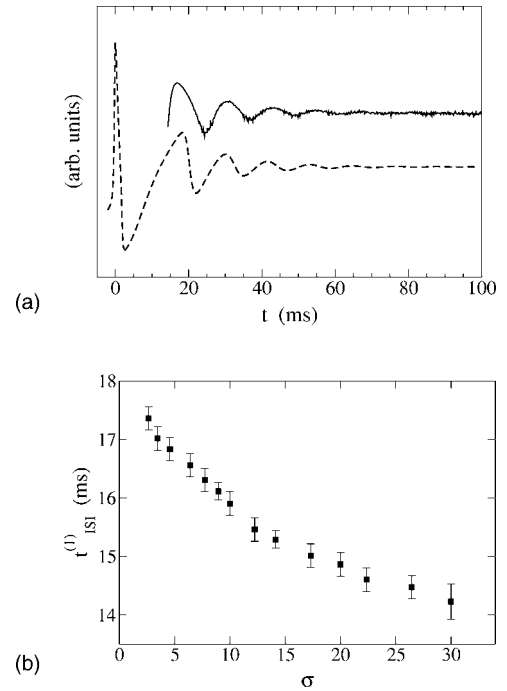


FIG. 4. (a)  $P_{ISI}(t)$  obtained by the stochastic input (3) with  $\sigma = 4.6$  (continuous curve) and the potential output  $V(t)$  following a step current stimulation (14) (dashed line). The position of the spike has been shifted to  $t=0$  and the action potential has been rescaled to better reveal the relaxation oscillations. (b)  $t_{ISI}^{(1)}$  as a function of  $\sigma$ . The error bars correspond to the histogram resolution employed to estimate  $P_{ISI}(t)$ . Data refer to  $\bar{I} = 6.15 \mu\text{A}/\text{cm}^2$ .

$$I(t) = \begin{cases} 0 & \text{if } t \leq 0, \\ \bar{I} & \text{if } t > 0, \end{cases} \quad (14)$$

and registered the shape of the output  $V(t)$ . As shown in Fig. 4(a) (dashed line), the HH model responds emitting one or more action potentials followed by damped oscillations. The first oscillation of period  $T_{nl}$  has a clear nonlinear character, while we have verified that the angular frequency  $2\pi/T_l$  describing the subsequent oscillations corresponds to the imaginary part of the complex conjugate Floquet eigenvalues associated to the stable fixed point. Therefore the latter solutions can be completely characterized within a linear stability analysis of model ((1),(2)).

To better compare the periods of the relaxation oscillations with the measured positions of the first (respectively second) peak  $t_{ISI}^{(1)}$  (respectively  $t_{ISI}^{(2)}$ ) of the ISI distribution, we have registered the temporal interval separating the peak of the action potential and the first subsequent maximum  $T_{nl}$  and corrected (increased) these values by the corresponding rise time needed to reach the detection threshold  $\Theta$ . As shown in Fig. 5, the comparison of  $t_{ISI}^{(1)}$  with the corrected values  $\tilde{T}_{nl}$  is very good for  $0 \leq \bar{I} \leq 5 \mu\text{A}/\text{cm}^2$ . Moreover, by approaching  $I_{SN}$  we observe that  $\tilde{T}_{nl} \rightarrow 1/\nu_c$  (where  $\nu_c$  is the frequency of the spike train limit cycles emerging at the saddle-node transition). For completeness we have also verified that the other peaks observed in the distribution  $P_{ISI}(t)$

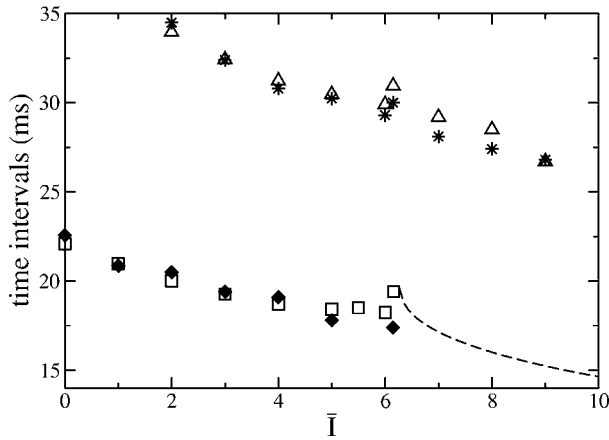


FIG. 5. Positions of the peaks of the distribution  $P_{ISI}(t)$  as a function of the average current  $\bar{I}$  for low noise: first peak  $t_{ISI}^{(1)}$  (filled diamonds) and second peak  $t_{ISI}^{(2)}$  (asterisks). For comparison the time intervals separating the induced spike from the maximum associated to the first (nonlinear) oscillation  $\tilde{T}_{nl}$  (empty squares) and to the second (linear) oscillation  $\tilde{T}_{nl}+T_l$  (empty triangles) are shown. The periods  $1/\nu_c$  of the regular spike trains emerging above  $I_{SN}$  are also plotted (dashed line). The data for  $t_{ISI}^{(1)}$  and  $t_{ISI}^{(2)}$  have been obtained for  $\sigma \approx 2.6-10$ .

are related to the subsequent linear oscillations of period  $T_l$  shown in Fig. 4(a) (dashed line). In particular, we concentrated on the second peak  $t_{ISI}^{(2)}$  and compared it with  $\tilde{T}_{nl}+T_l$ , also this time the agreement is quite good (see Fig. 5)<sup>3</sup>. In general for the  $m$ th peak we expect that a good approximation of its position will be given by  $\tilde{T}_{nl}+(m-1)T_l$ , and this is indeed verified as shown in Fig. 4(a).

The damped oscillations following a spike induce a modulation in the degree of excitability of the model, or analogously a modulated effective threshold for spike elicitation. Indeed a  $P_{ISI}(t)$  quite similar to that displayed in Fig. 4(a) was obtained by Wilbur and Rinzel by considering a leaky integrate-and-fire model with a threshold evolving dynamically in time [31].

So far we limited ourselves to low values of noise variance, by increasing  $\sigma$  we expect that the position of the first peak will be shifted to smaller values. Due to stronger noise fluctuations, after the emission of a spike a second spike can be elicited even before the subsequent relaxation oscillation of  $V(t)$  reaches its maximum value. This tendency of  $t_{ISI}^{(1)}$  to decrease with  $\sigma$  is illustrated in Fig. 4(b).

## 2. Firing activated by noise

In the first part of this subsection our analysis has been devoted to relatively short ISIs, however, the exponential tail present in  $P_{ISI}(t)$  [see Fig. 3(a)] is extremely relevant since it gives the main contribution to the average firing rate  $\nu_{out}$  of the neuron. As already mentioned, this long lasting tail should be related to some sort of activation process.

<sup>3</sup>Above the saddle-node transition  $\bar{I} > I_{SN}$  the position of the second peak has been estimated as  $1/\nu_c + T_l$ .

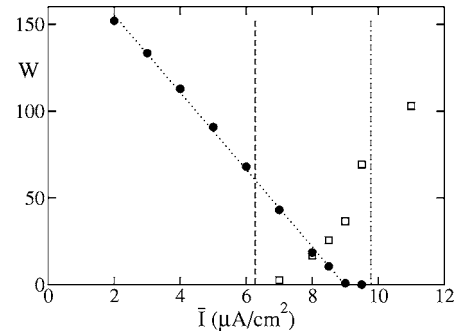


FIG. 6. Activation barrier heights  $W$  as a function of the average input current for the silent state  $W_S$  (filled circles) and the oscillatory state  $W_O$  (empty squares). The vertical dashed (respectively dot-dashed) line indicates the position of  $I_{SN}$  (respectively  $I_{HB}$ ). A linear fitting to  $W_S$  in the interval  $2 \mu\text{A}/\text{cm}^2 \leq \bar{I} \leq 9 \mu\text{A}/\text{cm}^2$  is also shown as a dotted line.

An activated firing can arise in this regime due to the competition between the tendency of the HH dynamics to relax towards its stable fixed point  $[V_{rest}(\bar{I})]$  and noise fluctuations that instead lead the system towards an excitation threshold (note, however, that there is no fixed threshold in the HH-model [1]). Therefore, the dynamics of  $V(t)$  resembles the overdamped dynamics of a particle in a potential well under the influence of thermal (stochastic) fluctuations [32]. Due to the activation process the membrane potential can be driven towards the excitation threshold with an average escape time given by Kramers expression [32]

$$T_e \propto e^{W_S/\sigma^2}, \quad (15)$$

where  $W_S$  plays the role of an energy barrier and  $\sigma^2$  of an effective temperature of the bath. This behavior is indeed verified for small  $\sigma$ -values as shown in the inset of Fig. 2. Therefore we expect that for  $\sigma < \sigma_c \equiv \sqrt{W_S}$  ( $\sigma_c \approx 9.64$  for  $\bar{I} = 5 \mu\text{A}/\text{cm}^2$ ) the dynamics can be characterized as an activation process, while for  $\sigma^2$  larger than the barrier value the dynamics should be mainly diffusive. A further indication that for low noise the dynamics is essentially Poissonian is given by the fact that  $R \approx 1$  for  $\sigma < \sigma_c$ . We have estimated  $W_S$  for various values of the average current for  $\bar{I} < I_{HB}$  and a linear decrease of the barrier height with  $\bar{I}$  is clearly observable in Fig. 6, except in direct proximity of  $I_{HB}$ . Moreover (as expected)  $W_S \rightarrow 0$  approaching  $I_{HB}$  where the fixed point loses its stability via a subcritical Hopf bifurcation<sup>4</sup>.

To gain some deeper insight into the role of noise fluctuations in eliciting a spike, we have estimated the STAP  $V(t)$  and the STAF  $q(t)$  for sufficiently long ISIs and for small  $\sigma$ . As shown in Fig. 7,  $q(t)$  and  $V(t)$  exhibit oscillations of pe-

<sup>4</sup>The average escape times  $T_e$  have been estimated directly as  $1/\nu_{out}$  for  $\bar{I} < I_{SN}$  since at sufficiently low noise the activation is the prevailing mechanism in this regime; above  $I_{SN}$  where there is a coexistence of a stable limit cycle with a stable fixed point these times have been measured as the residence times  $T_S$  in the silent state (i.e., in proximity of the fixed point).

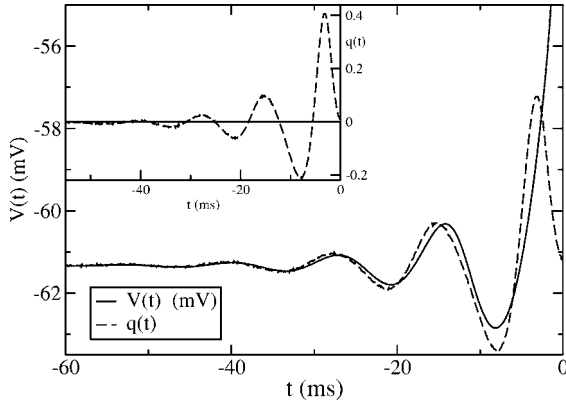


FIG. 7. STAF  $q(t)$  (dashed line) and STAP  $V(t)$  (solid line) preceding the emission of a spike. At time  $t=0$  the potential overcomes the detection threshold  $\Theta$ . Both quantities have been defined by employing a time window  $\Delta T=0.1$  ms and have been averaged only over ISIs longer than 150 ms. The data refer to  $\bar{I}=5 \mu\text{A}/\text{cm}^2$  and  $\sigma=5.7$ . For a better comparison  $q(t)$  has been shifted and amplified by a factor 10, the original function is displayed in the inset.

riod  $\approx T_l$  preceding the spike emission and these oscillations are almost in phase, apart from a small delay in the response of  $V(t)$  with respect to the input noise. This indicates that the potential follows the current oscillations and that the emission of a spike (for long ISIs) is commonly triggered by the excitation of linear subthreshold oscillations around the rest potential. Therefore the neuron in proximity of the rest state acts as a sort of selective filter since it responds (by emitting a spike) with higher probability when excited with a specific input frequency ( $\approx 1/T_l=61-88$  Hz for  $0 \leq \bar{I} \leq I_{SN}$ ). This result agrees with a previous analysis reported in [21], where it has been shown that a silent HH neuron, subjected to a sinusoidal current, optimally resonates when forced with a frequency linearly correlated with  $1/T_l$ .

### 3. High noise limit

As already mentioned, for sufficiently high noise the probability density distribution of the ISIs reduces to an inverse Gaussian. The reason is that for  $\sigma \gg \sigma_c$  the “potential well” surrounding the stable fixed point becomes irrelevant for the dynamics due to the amplitude of the noise fluctuations, whose effect on the dynamics of the neuron are twofold: a constant current  $\bar{I}$  driving the system plus a stochastic (Gaussian) term with zero average. Therefore we can assume that the dynamics of the membrane potential is determined by a Langevin equation with a drift term. The distribution of the first passage time from a certain threshold, in the presence of a reset mechanism to a fixed rest potential, is given by the well known inverse Gaussian distribution [1,30]

$$f(t) = \frac{\alpha}{\sqrt{2\pi\beta t^3}} e^{-[(t-\alpha)^2]/(2\beta t)}, \quad (16)$$

where  $\alpha=A_{ISI}$  and  $\beta=S_{ISI}^2/A_{ISI}$ . The good agreement shown in Fig. 3(c) confirms that the mechanism leading to repetitive firing in the high noise limit can be indeed schematized as a Wiener process plus drift.

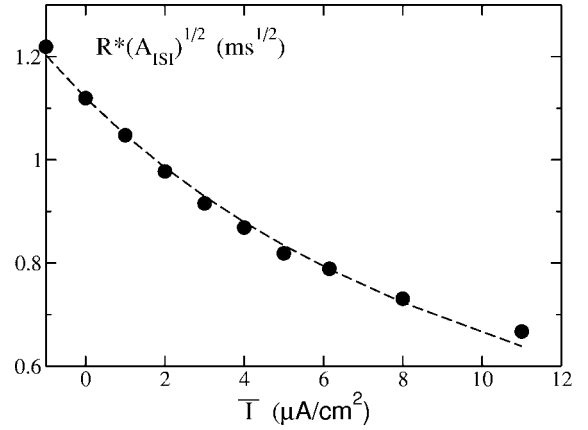


FIG. 8.  $R \times \sqrt{A_{ISI}}$  (filled circles) versus  $\bar{I}$ , the dashed line is a best fit to the data of the form  $a/(\bar{I}+I_0)$  with  $a=16.35 \text{ ms}^{1/2} \mu\text{A}/\text{cm}^2$  and  $I_0=14.59 \mu\text{A}/\text{cm}^2$ . The data refer to  $\sigma=100$ .

Moreover, by assuming that the drift is proportional to  $\bar{I}$  and the amplitude of the effective noise to  $\sigma$  one obtains the following dependence for the ISI coefficient of variation [1]

$$R \propto \frac{\sigma}{(\bar{I} + I_0) \sqrt{A_{ISI}}}, \quad (17)$$

where  $I_0$  is a parameter. For fixed noise variance,  $R \times \sqrt{A_{ISI}}$  should then be inversely proportional to  $\bar{I} + I_0$  as indeed verified for  $\sigma=100$  in Fig. 8.

## B. Coexisting coherence resonances

In the silent regime we have encountered two coexisting coherence resonance phenomena. The first one is related to the existence of an optimal noise level for the regularization of the output spike trains and it corresponds to the effect previously reported in [20,21]. The second coherence effect can only be detected by considering the membrane potential dynamics, not being associated with spikes, but instead with the excitation of quite regular sequences of subthreshold oscillations occurring at small noise variances.

### 1. Coherence of the emitted spike trains

At intermediate noise levels the  $P_{ISI}(t)$  reduces its exponential tail and begins to assume the shape of an inverse Gaussian distribution [see Fig. 3(b)]. Therefore, the activation mechanism responsible for the firing is gradually substituted by another stochastic mechanism resembling a Wiener process with drift. In correspondence to the transition from one kind of stochastic process to the other a regularization of the output signal is observed: this phenomenon is known as *coherence resonance* [13] and has already been reported for various neuronal models. Our aim in the present subsection is to give a more detailed characterization of the CR phenomenon in terms of commonly used indicators of coherence [14], like the coefficient of variation  $R$  and the correlation time  $\tau_c$ , but also in terms of the saturated conditional entro-

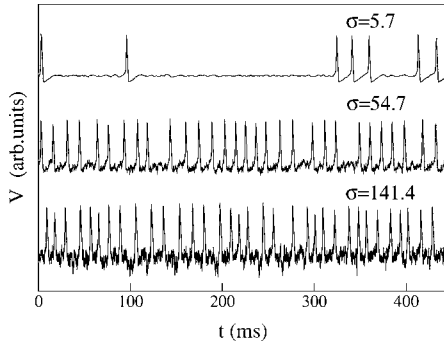


FIG. 9. Membrane potentials  $V(t)$  for various levels of noise  $\sigma$  in the silent regime at  $\bar{I}=5 \mu\text{A}/\text{cm}^2$ .

pies  $h_A$ , not previously employed in this context.

Let us first examine the signals displayed in Fig. 9 for  $\bar{I}=5 \mu\text{A}/\text{cm}^2$ . At low  $\sigma$ -values one observes rare spikes induced by the activation mechanism, while for increasing noise the train becomes more and more regular and finally at high  $\sigma$ -values the noise begins to modify even the relative refractory times.

A first quantitative evidence of coherence resonance can be given in terms of  $R$ : at low  $\sigma$  this quantity tends to one as expected for Poissonian processes, indeed  $R$  reaches a value slightly greater than one due to the multimodal structure of the  $P_{ISI}(t)$ ; for increasing  $\sigma$  the  $S_{ISI}$  decreases faster than  $A_{ISI}$  since the diffusive nature of the process begins to prevail over the activation effects [exemplified by a Poissonian distribution for  $P_{ISI}(t)$  with  $S_{ISI}=A_{ISI}$ ]. The behavior of  $R$  at large  $\sigma$ -values is given by the expression (17) and since  $A_{ISI}$  slightly decreases for large noise amplitude the coefficient of variation turns out to be an increasing function of  $\sigma$ . A minimum of  $R$  is found at intermediate noise levels due to the predominance of two different mechanisms at the origin of spiking in two opposite limits: activated barrier crossing in the limit  $\sigma \ll \sigma_c$  and diffusive motion with drift in the opposite limit  $\sigma \gg \sigma_c$ . Indeed, as shown in Fig. 10 a minimum is attained for  $\sigma \equiv \sigma_R \approx 55$  for  $\bar{I}=5 \mu\text{A}/\text{cm}^2$ .

A second striking evidence of coherence resonance is given by a maximum in the correlation time  $\tau_c$  estimated directly by integration of the squared autocorrelation function of the signal according to Eq. (10). This maximum oc-

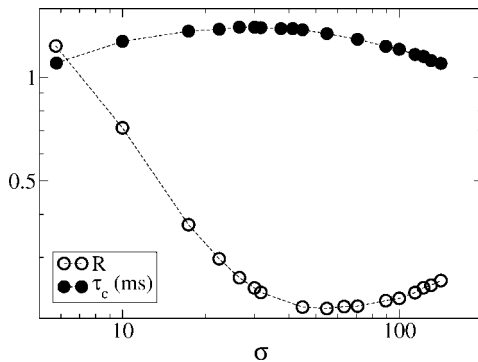


FIG. 10.  $\bar{I}=5 \mu\text{A}/\text{cm}^2$ : coefficient of variation  $R$  (empty circles) and correlation time  $\tau_c$  (filled circles) as a function of  $\sigma$ .

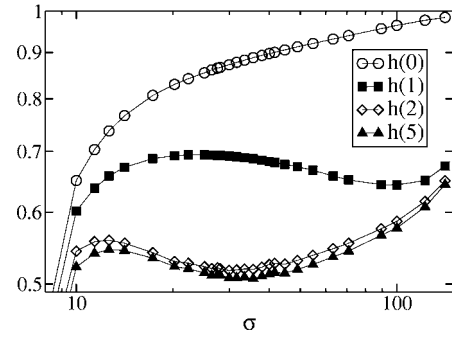


FIG. 11. Conditional entropies  $h(N)$  as a function of  $\sigma$  for various word lengths  $N$ . The data have been obtained for  $\bar{I}=5 \mu\text{A}/\text{cm}^2$  with a resolution of  $\Delta t=5$  ms.

curr for a value smaller than that obtained for  $R$ , i.e.,  $\sigma \equiv \sigma_\tau \approx 30$  for  $\bar{I}=5 \mu\text{A}/\text{cm}^2$ .

As previously suggested for SR [22], dynamical entropies are indicators appropriate to characterize the degree of unpredictability of the output of a certain nonlinear system, therefore we expect that they should be useful also in the present context. In Fig. 11 the conditional entropies  $h(N)$  are reported for increasing word length  $N$  at  $\bar{I}=5 \mu\text{A}/\text{cm}^2$ . These quantities saturate to their asymptotical values  $h_A$  for  $N=5$ , thus indicating that the present dynamics can be reproduced in terms of a Markovian process of order five with a temporal memory  $\approx 5 \times \Delta t=25$  ms. Since for this current value  $A_{ISI}$  varies between 17 ms and 11 ms for  $20 < \sigma < 150$ , this means that in order to recover all the transmitted information it is sufficient to record from two to three successive spikes. Similar to what has been reported in [22]  $h_A$  exhibits a non-monotonic behavior characterized by a rapid initial growth at small  $\sigma$  followed by a decrease and a minimum at intermediate noise ( $\sigma \equiv \sigma_h \approx 33$ ). Initially the signal is extremely regular, being essentially a sequence of zeros in the absence of spikes, then the noise tends to randomize the system and this induces a rapid increase. Finally, the signal regularizes at finite  $\sigma$  and this leads to the occurrence of a minimum in the asymptotic entropies.

We can safely affirm that the three employed indicators agree in indicating a clear coherence resonance effect at the considered current  $\bar{I}=5 \mu\text{A}/\text{cm}^2$ . Furthermore, we performed a similar analysis at various current  $\bar{I}$  in the silent and in the bistable regime and the corresponding values  $\sigma_R$ ,  $\sigma_h$ ,  $\sigma_\tau$  are shown in Fig. 12. For all indicators the optimal amount of noise needed to observe CR decreases for increasing current. However, while  $\sigma_R$  and  $\sigma_h$  seem not to vary dramatically in the examined range,  $\sigma_\tau$  decreases noticeably approaching the SN bifurcation. This behavior seems to be due to the fact that the signal autocorrelation function does not only register coherence effects associated to the ISIs, but also those related to the subthreshold oscillations occurring at quite low noise (as reported in the next subsection). The interaction between these two resonances leads to the enhanced decrease of  $\sigma_\tau$ , somehow the ISI resonance is entrained by the second one and shifted towards small  $\sigma$ . Other indications that the signal becomes more and more correlated approaching  $I_{SN}$  are given by the corresponding increase of the maximal correla-

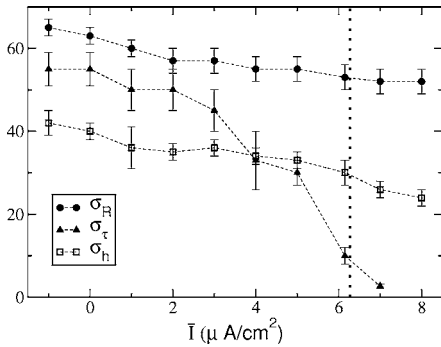


FIG. 12. Optimal noise standard deviations corresponding to coherence resonance versus  $\bar{I}$  for the three considered indicators: namely,  $\sigma_R$  (filled circles),  $\sigma_\tau$  (filled triangles), and  $\sigma_h$  (empty squares). The vertical dotted line indicates  $I_{SN}$ , while the dashed lines are guides for the eyes.

tion time and by the decrease of the minimum of  $R$  and of  $h_A$  (all measured at the resonance). This scenario is consistent with the fact that the activation barrier  $W_S$  separating the rest state from the excited state also decreases with  $\bar{I}$  and therefore the latter becomes more accessible at lower noise variances.

## 2. Coherence of the subthreshold oscillations

Let us now discuss in more detail the origin of the second coherence resonance observed at very low noise variance. In Fig. 13 the behavior of the correlation time  $\tau_c$  as a function of  $\sigma$  is shown for  $\bar{I}=4 \mu\text{A}/\text{cm}^2$  in a wider range of noise with respect to the data shown in Fig. 10. In that figure the examined noise range was restricted to values for which the statistics of emitted spikes was sufficiently rich to ensure a meaningful definition of  $R$ . In Fig. 13(a)  $\tau_c$  reveals two clear maxima: the higher one located at  $\sigma \approx 3$  and the lower one at  $\sigma \approx 33$ . The origin of the first peak can be understood as follows: for  $\sigma < 3$  almost no spikes are emitted by the neuron, however, the increase of noise tends to stimulate series of subthreshold oscillations that are more and more correlated; for  $\sigma > 3$  the statistics of the emitted spikes begins to be no more negligible and the occurrence of rare spikes tends to decorrelate the signal leading to a decrease of  $\tau_c$ . By further increasing the noise variance the signal begins to be characterized by a sequences of spikes, therefore the autocorrelation function starts to register essentially the correlation of these events and  $\tau_c$  reveals a second peak related to the regularization of the spike trains, this is the coherence phenomenon previously discussed.

The transition from one dynamical regime to the other can be better understood by examining the autocorrelation function of  $V(t)$  for various values of  $\sigma$ . As shown in Fig. 13(b), for  $\sigma \approx 3$  the autocorrelation function  $C(t)$  reveals oscillations of period  $\approx T_I$ , while at  $\sigma \approx 9.7$  the maxima of  $C(t)$  are located in correspondence with multiples of  $t \approx t_{ISR}^{(1)}$ . In between these two values there is a transition from an output signal dominated by the subthreshold oscillations to a signal characterized by trains of spikes, this transition can be located at  $\sigma \approx 4.5$ , since at this value  $C(t)$  exhibits, at the first

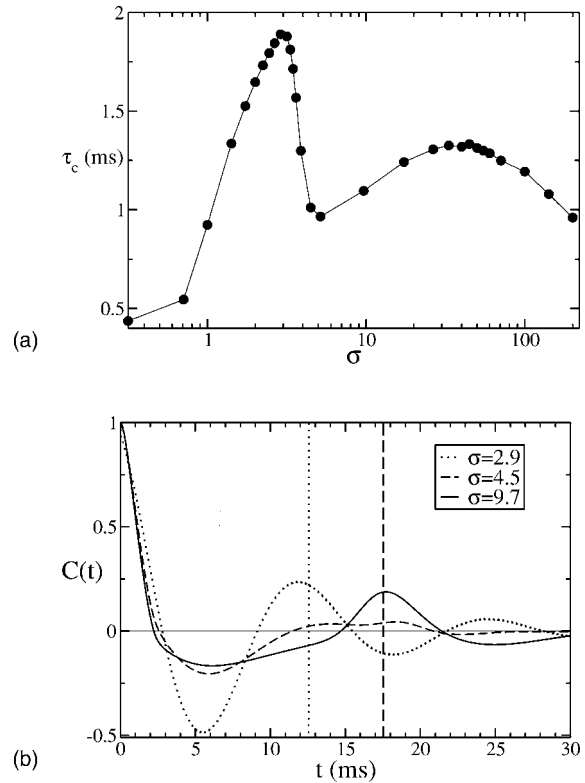


FIG. 13.  $\bar{I}=4 \mu\text{A}/\text{cm}^2$ : (a)  $\tau_c$  (filled circles) as a function of  $\sigma$ , the solid line is a guide for the eyes; (b) autocorrelation functions  $C(t)$  for three different noise values (namely  $\sigma=2.9, 4.5$  and  $9.7$ ), the vertical dotted line indicates the period  $T_I$ , while the vertical dashed line refers to  $t_{ISR}^{(1)}$  for  $\sigma=9.7$ .

oscillation, two maxima, one located at  $t \approx T_I$  and one at  $t \approx t_{ISR}^{(1)}$ .

To summarize, for the HH model in the silent regime two kind of coherence resonances can be observed, one at quite low noise related to the excitation of subthreshold oscillations around the rest state and another one at higher noise due to the regularization of successive  $ISIs$  associated to the spikes emitted by the neuron. Obviously, since the first resonance is not related to spike occurrence it cannot be revealed by  $R$  or by  $h$ , but only by  $\tau_c$ .

## IV. BISTABLE REGIME

In the bistable regime the modifications of the shape of the  $ISI$  distributions due to the effect of noise resemble those found in the silent regime, apart from very low noise variances (see Fig. 14). As shown in Fig. 14(a), in this latter case one observes a quite pronounced peak corresponding to  $1/\nu_c$  followed by smaller multi-peaks and an exponential tail. This reflects the fact that the dynamics due to the noise switches back and forth between the two coexistent states: oscillatory and silent [cf. the time evolution of the membrane potential reported in Fig. 15, in particular at  $\sigma=3.2$  (for  $\bar{I}=8 \mu\text{A}/\text{cm}^2$ )]. This dynamical behavior is reminiscent of the motion of one particle in a double well subjected to thermal fluctuations. Therefore, the residence times in the two states

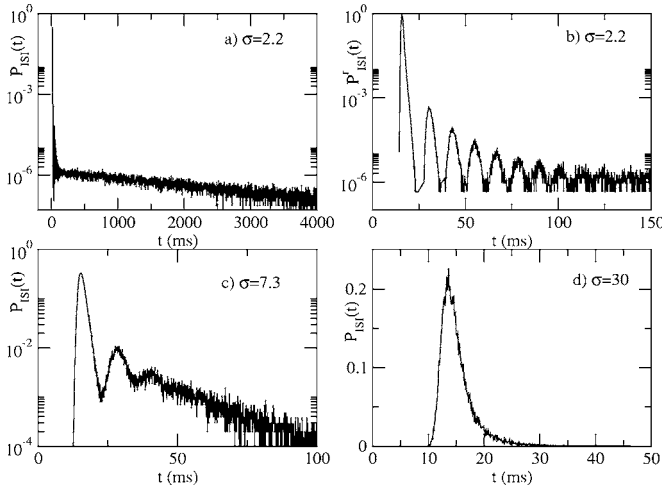


FIG. 14.  $P_{ISI}(t)$  in the bistable regime at  $\bar{I}=8 \mu\text{A}/\text{cm}^2$ .  $P_{ISI}(t)$  is displayed for various values of the noise:  $\sigma=2.2$  (a),  $\sigma=7.3$  (c), and  $\sigma=30$  (d). Additionally in (b)  $P'_{ISI}(t)$  is shown for  $\sigma=2.2$ .

should be related with the noise amplitude by a Kramers relationship in the standard manner

$$T_x \propto e^{W_x/\sigma^2}, \quad (18)$$

where  $x=S$  for the silent state and  $x=O$  for the oscillatory state. Moreover, the distributions of  $T_S$  (respectively  $T_O$ ) should be Poissonian due to the stochastic nature of the jumping from one state to the other. In order to verify Eq. (18) we have estimated the times  $T_S$  and  $T_O$  as a function of  $\sigma$  for small values of this parameter. The data, displayed in Fig. 16, confirm that in the low noise limit both times can be described in terms of an activation process induced by noise fluctuations. Moreover, barriers  $W_O$  and  $W_S$  have been estimated for various currents and are reported in Fig. 6. For  $I_{SN} < \bar{I} < 8 \mu\text{A}/\text{cm}^2$  the most stable state is the fixed point, while above  $I=8 \mu\text{A}/\text{cm}^2$  the stability of the oscillatory state prevails.

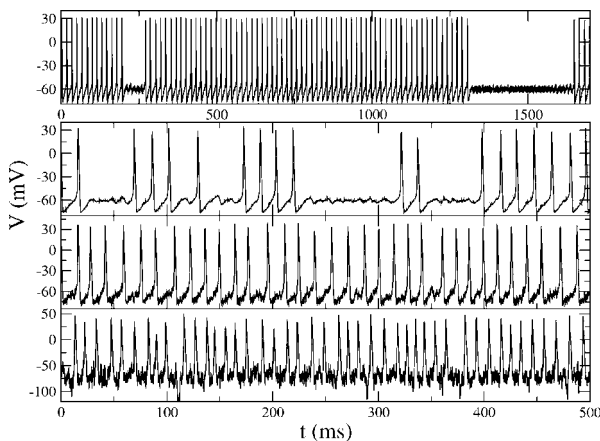


FIG. 15. Membrane potential  $V(t)$  evolution in time for various values of the noise variance. The top signal refers to  $I=8 \mu\text{A}/\text{cm}^2$  and  $\sigma=3.2$ , the other three curves correspond (from top to bottom) to  $\sigma=6.8, 38.7$ , and  $141.6$  and  $I=7 \mu\text{A}/\text{cm}^2$ .

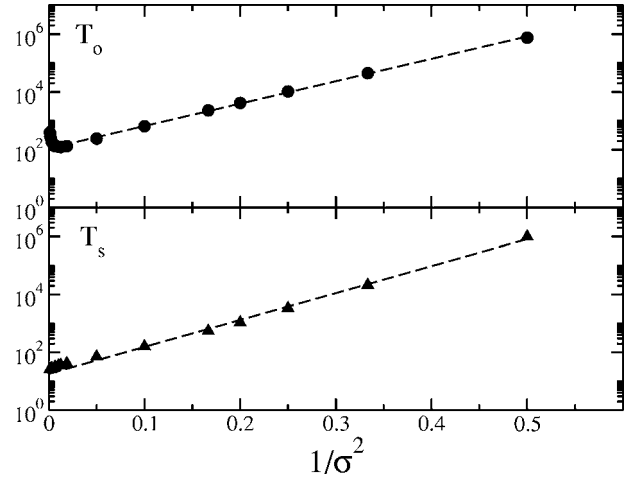


FIG. 16. Residence times  $T_O$  and  $T_S$  as a function of  $1/\sigma^2$  for low noise variance values: the dashed lines are fits to the numerical data with expression (18) for  $\sigma \leq 4$ , the corresponding barriers are  $W_S=21.4 \pm 0.5$  and  $W_O=17.9 \pm 0.3$ . All data refer to  $\bar{I}=8 \mu\text{A}/\text{cm}^2$ .

Let us now come back to the  $P_{ISI}(t)$  for  $\sigma=2.2$ , in this case we have estimated the distributions of the ISIs during the oscillatory state only, let us term this probability distribution as  $P'_{ISI}(t)$ . This distribution, reported in Fig. 14(b), reveals a multimodal structure. While the first peak corresponds to  $\approx 1/\nu_c$ , the other peaks are related to the linear damped oscillations towards the fixed point, i.e.,  $t_{ISI}^{(k+1)} - t_{ISI}^{(k)} \approx T_l$  for  $k \geq 1$ . The origin of this multimodal structure can be understood by comparing the STAF  $q_I(t)$  preceding the emission of a spike for intermediate ISI-values (namely for ISI durations corresponding to the second and third peak of the distribution) with the STAF  $q_L(t)$  associated with long ISIs falling in the exponential time tail. Analogously to what we observed in the silent regime  $q_L(t)$  reveals oscillations of a period  $\approx T_l$ , indicating that the neuron will return to fire, once entered in the silent state, mainly when stimulated via current oscillations of the proper period and in phase with  $V(t)$  oscillations (see Fig. 7). As shown in Fig. 17,  $q_I(t)$  has a quite peculiar behavior, it also exhibits oscillations of period  $\approx T_l$ , but these oscillations are in antiphase with respect to

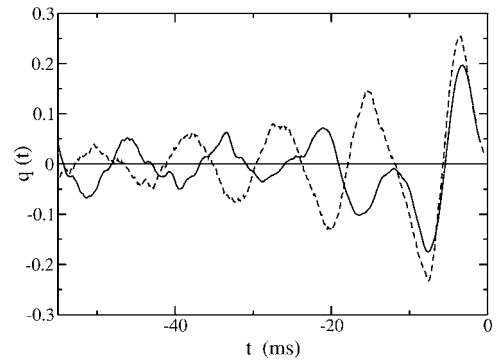


FIG. 17. STAF for long ISIs  $q_L(t)$  (dashed line) and intermediate ISIs  $q_I(t)$  (solid line) for  $\bar{I}=8 \mu\text{A}/\text{cm}^2$  and  $\sigma=3.2$ .  $q_L(t)$  has been estimated by averaging over  $ISI > 70$  ms, while  $q_I(t)$  refer to  $25 \text{ ms} < ISI < 70$  ms.

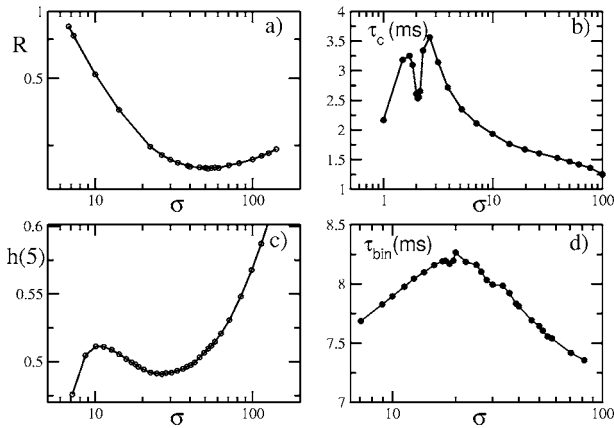


FIG. 18. Regime of bistability ( $\bar{I}=7 \mu\text{A}/\text{cm}^2$ ):  $R$  (a),  $\tau_c$  (b),  $h_A=h(5)$ , (c), and  $\tau_{bin}$  (d) as a function of  $\sigma$ .

those of  $q_L(t)$ , apart from the last two preceding the firing of the neuron. This means that, once entered in the oscillatory state, the neuron can become silent only if a series of current oscillations [in antiphase with respect to the damped oscillations of  $V(t)$  following a spike] inhibit repetitively spike emission allowing a sufficient decrease of  $V(t)$  leading the system in the attraction basin of the rest state. If by chance one of these oscillations returns in phase with  $V(t)$  (during the relaxation) the neuron will fire immediately after (as shown in Fig. 17). This is the mechanism at the origin of the various peaks present in  $P_{ISI}(t)$  at low noise values, some indications consistent with this scenario have been recently reported in Ref. [8].

As far as CR is concerned, a clear resonance is observable by inspecting the dependence of  $R$  and the saturated  $h_A$  as a function of noise intensity for  $\bar{I}=7 \mu\text{A}/\text{cm}^2$  (see Fig. 18). On the other hand,  $\tau_c$  exhibits two almost coinciding maxima at very low noise: one due to subthreshold oscillations at  $\sigma=1.8$  and the other one related to ISI coherence at  $\sigma_\tau=2.6$ . At higher currents the two maxima merge and they are no more distinguishable one from the other. In order to understand if a ISI coherence effect is still clearly discernible at the level of correlation functions we have estimated the time  $\tau_{bin}$  defined in terms of  $C_{bin}$  (13). This quantity, which is not influenced by the subthreshold oscillations, shows a clear maximum at  $\sigma=20$  [see Fig. 18(d)]. Since  $C_{bin}$  and  $h_A$  measure both dynamical features of the ISI sequence we expect that they should give similar information, indeed for this current  $\sigma_h=26\pm 2$ . These results seem to indicate that the information reduction needed to pass from the signal to the ISIs allows to better single out the “standard” coherence phenomenon in this regime. By further increasing the current the only indicator that continues to signal a coherence resonance effect is  $R$ , while at  $\bar{I}=9 \mu\text{A}/\text{cm}^2$  the minimum present in  $h$  becomes a shoulder and also  $\tau_{bin}$  does not exhibit maxima at intermediate noise. The main difference between the dynamics at  $\bar{I}=7 \mu\text{A}/\text{cm}^2$  and  $\bar{I}=9 \mu\text{A}/\text{cm}^2$  is related to the fact that the oscillatory state becomes more stable than the silent state at this latter current (i.e.,  $W_O > W_S$ ). To summarize, the coexistence of two coherence resonance is observed also in the bistable regime until the fixed point remains the most stable solution (i.e., for  $\bar{I} \leq 8 \mu\text{A}/\text{cm}^2$ ).

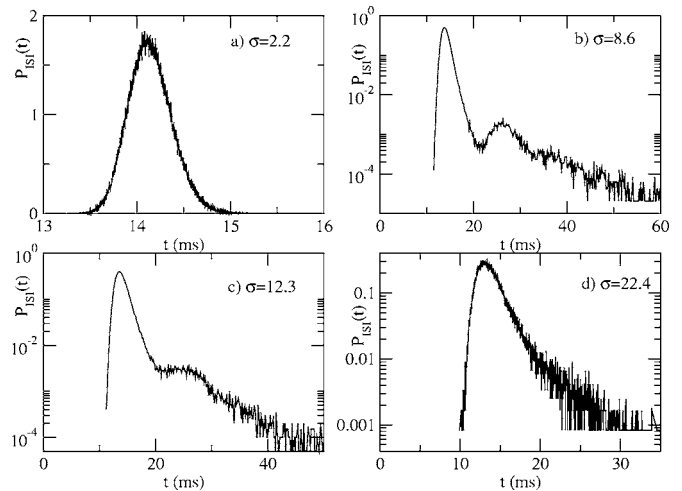


FIG. 19.  $P_{ISI}(t)$  corresponding to  $\bar{I}=11 \mu\text{A}/\text{cm}^2$  for various  $\sigma$ -values:  $\sigma=2.2$  (a), 8.6 (b), 12.3 (c), and 22.4 (d).

## V. REPETITIVE FIRING REGIME

Above  $I_{HB}$  the system is in a stable regime of repetitive firing if subjected to a constant current. As we can see from Fig. 19, the noise has a different effect this time. In particular, for sufficiently small  $\sigma$  we observe that  $P_{ISI}(t)$  is essentially a Gaussian centered around the repetitive firing period  $1/\nu_c$  [see Fig. 19(a)]. Initially for  $1 < \sigma < 3$ ,  $S_{ISI}$  increases linearly with  $\sigma$ , as expected for additive noise of sufficiently small intensity. Upon further increasing the variance of the noise, the distribution becomes again multimodal [as shown in Fig. 19(b)] with peaks located at integer multiples of  $1/\nu_c$ , but this time the activation tail is almost absent. The multi-peak structure (mainly limited to two peaks only) is due to the fact that sometimes the neuron fails to emit a spike at  $1/\nu_c$  because of a current fluctuation in antiphase with the suprathreshold oscillations of the membrane potential. This mechanism is analogous to the one already described in the previous section to explain the multi-peaks observed in the bistable regime. At larger  $\sigma$  the second peak reduces to a shoulder [see Fig. 19(c)] and then  $P_{ISI}(t)$  converges toward an inverse Gaussian.

In this regime the only indicator giving evidence of CR is the coefficient of variation  $R$ , while for  $\sigma \rightarrow 0$  the correlation time  $\tau_c$  diverges to infinite, since the system converges to a stable limit cycle, and the conditional entropies do not exhibit any relative minimum. As shown in Fig. 20,  $R$  has a maximum at  $\sigma=12.3$  (for  $R \approx 0.19$ ) followed by a minimum at  $\sigma=30$  (corresponding to  $R \approx 0.17$ ). However, due to the very limited variation of  $R$ , it is difficult to appreciate from the signal evolution some difference between  $\sigma=12.3$  and 30. A similar effect of maximal spike train incoherence was observed for a leaky integrate-and-fire model with an absolute refractory period for suprathreshold base current [17]. In that case a maximum occurs at intermediate noise values since perfectly regular spiking was found for vanishing noise and in the large noise limit. In our model the maximum in  $R$  is related to the emergence of the multi-peak structure of  $P_{ISI}(t)$ . In the limit  $\sigma \rightarrow 0$  we observe regular spiking (i.e.,

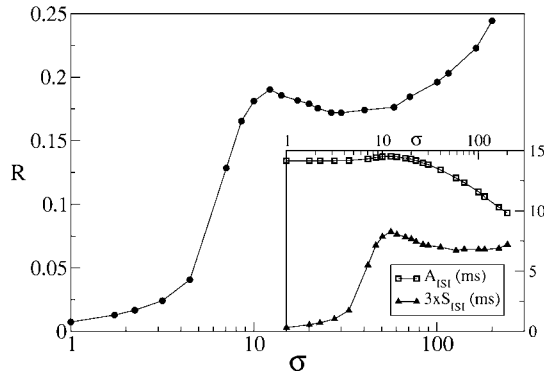


FIG. 20.  $R$  (filled circles) versus  $\sigma$  for  $\bar{I}=11 \mu\text{A}/\text{cm}^2$ . In the inset are reported  $A_{ISI}$  (empty squares) and  $S_{ISI}$  (filled triangles) for the same current.

$R \rightarrow 0$ ), the introduction of noise in the system initially leads to small irregularities in the spiking (reflected in the linear increase of  $S_{ISI}$  with  $\sigma$ ), and then to the emergence of the second peak in  $P_{ISI}(t)$ , that induces an abrupt growth in the  $S_{ISI}$ -value (as shown in the inset of Fig. 20) and also in  $R$ . At higher noise levels ( $\sigma > 23$ ) the dynamics reduces essentially to a Wiener process plus drift, this implies a merging of the two peaks associated with a simultaneous decrease of  $S_{ISI}$  followed by a saturation. The further randomization of the dynamics leads to a decrease of  $A_{ISI}$ , that tends to its asymptotic value, which is the refractory time. In addition, this behavior of  $A_{ISI}$  is responsible for the minimum of  $R$  at  $\sigma=30$  and for the successive growth consistent with Eq. (17).

VI. SUMMARY AND FINAL REMARKS

In the present paper we have studied the Hodgkin-Huxley model in the high-input regime subject to stochastic trains of uncorrelated inhibitory and excitatory kicks. Our analysis suggests that the specific shape of the time distribution of the arrival times play no role in this framework. Moreover, the response of the model is completely determined once the average and the variance of the stochastic input are given.

In the silent regime we have reported the coexistence of two coherence resonances: one corresponding to the regularization of the emitted spike trains at intermediate noise levels and the other one to the stimulation of subthreshold oscillations occurring at very low noise. All the employed indicators, namely the coefficient of variation, the signal and ISI correlation times, and the conditional entropies, are able to identify the first resonance, while the second one can be detected only by the autocorrelation time of the signal. Conditional entropies, used in the context of coherence resonance, turns out to be an effective indicator for coherence. Experimental evidences of a similar coexistence of two kinds of resonance has recently been reported in [33] for measurements performed on an electrochemical cell and numerically corroborated by simulations of a FitzHugh-Nagumo model. However, there are two differences with our analysis: in Ref. [33] the subthreshold signal was injected in the system together with the noise (therefore it is a stochastic resonance,

and not a coherence resonance) and the two resonances are both observable at the level of spike trains.

The dynamics in the bistable regime can be described by activated jumping processes across barriers between two stable solutions: namely, the oscillatory and silent state. The relative stability of the two dynamical regimes is ruled by the ratio of the corresponding barrier heights: until the fixed point solution remains the most stable state the observed dynamics resembles that in the silent regime. In the repetitive firing regime the only noticeable feature is related to a maximization of incoherence observed at a finite noise level.

Moreover, we have clarified the various mechanisms responsible for spike triggering and for ending repetitive firing. In particular, at relatively low noise the silent neuron can fire due to stochastic fluctuations via two mechanisms: one related to relaxation oscillations following a spike and another one associated with noise induced activation processes. The first mechanism lead to the multi peaked structure of the ISI distributions while the latter is responsible for the exponential tail. The presence of peaks in the  $P_{ISI}(t)$  suggests that the system, under the influence of stochastic inputs, can resonate when forced with specific frequencies corresponding to  $1/t_{ISI}^{(k)}$ , the main peak (due to nonlinear effects) being associated to frequencies in the  $\gamma$ -range [34] (namely, from 40 to 66 Hz for  $\bar{I} \in [0:9] \mu\text{A}/\text{cm}^2$ ), while the second one to lower frequencies (namely, from 30 to 37 Hz for the same interval of currents). Indeed these results can represent an explanation of recent findings [35], where clear stochastic resonance effects were observed in the range from 30 to 65 Hz for a Hodgkin-Huxley neuron subjected to Poisson distributed trains of EPSPs and IPSPs with periodically modulated rates plus a subthreshold harmonic signal. The authors [35] suggest that the origin of such SR should be related to sub-threshold oscillations, however, the corresponding frequencies (i.e.,  $61 \leq 1/T_l \leq 92$  Hz for  $\bar{I} \in [0:9] \mu\text{A}/\text{cm}^2$ ) are too high to match with the observed resonance. Once relaxed in the rest state the Hodgkin-Huxley neuron begins to act as a selective filter responding to current fluctuations with the same frequency of the linear subthreshold oscillations, in agreement with the analysis in [21].

In the bistable and repetitive firing regime the multimodal structure of  $P_{ISI}(t)$  at low noise is related to the periodicity of suprathreshold and (linear) subthreshold oscillations. Tonic firing states end when the neuron is stimulated with fluctuations in antiphase with respect to the internal oscillations. In the high noise limit the neuron dynamics in all the three examined regimes can be represented as a stochastic Wiener process plus drift.

In conclusion, we have shown that the Hodgkin-Huxley neuron in the high input regime displays a large variety of dynamical behaviors, thus rendering the study of its dynamics interesting *per se* and not only for its biophysical implication. The richness of the Hodgkin-Huxley dynamics is particularly pronounced in the silent regime for low input noise variance, where the response of the model resembles more the activity of cortical neurons, since it is characterized by an almost Poissonian distribution of interspike intervals [6]. Apart from this feature, in this regime the  $P_{ISI}(t)$  presents a multimodal structure indicating that the single neuron re-

sponse is particularly enhanced in correspondence to specific stimulation frequencies, thus possibly allowing for detection and transduction of a variety of input signals. Moreover, a network of such neuronal elements will have the capability to exhibit coherent and correlated activity over different time scales (mainly in the  $\gamma$  and  $\beta$ -ranges [34]), a property that is believed to be important for information encoding for cortical processing [36]. Indeed, it has been found [21] that a globally coupled Hodgkin-Huxley network subjected to stochastic inputs reveal, for sufficiently strong synaptic coupling, a collective synchronized rhythmic firing in a range of 40–60 Hz, induced via coherence resonance.

A point that has not been addressed in the present study and that deserves further investigation is the influence of the membrane time constant on the neuronal response. As already mentioned, for the Hodgkin-Huxley model the time constant is  $\approx 1$  ms, similar to that measured for the auditory brainstem neurons [37], while typically cortical neurons ex-

hibit constants ranging from 10 to 40 ms [2]. An increase of the time constant would alter the response of the neuron in the low noise limit (by reducing the activation period preceding spike emission) but this should have a limited effect on the dynamics at intermediate and high noise variance.

As future developments of the present work, we plan to investigate the role played by correlations among the synaptic inputs in enhancing or depressing the coherence effects here discussed.

#### ACKNOWLEDGMENTS

We acknowledge useful discussions with V. Beato, S. Lepri, B. Lindner, R. Livi, A. Politi, L. Schimansky-Geier, and R. Zillmer. One of us (T.K.) has been supported by the Marie Curie Individual Intra-European Fellowship “DEAN,” Project No 011434.

- 
- [1] H. C. Tuckwell, *Introduction to Theoretical Neurobiology*, (Cambridge University Press, New York, 1988).
- [2] C. Koch, *Biophysics of Computation* (Oxford University Press, New York, 1999).
- [3] W. Gerstner and W. Kistler, *Spiking Neuron Models* (Cambridge University Press, Cambridge, 2002).
- [4] A. L. Hodgkin and A. F. Huxley, *J. Physiol. (London)* **117**, 500 (1952).
- [5] C. Meunier and I. Segev, *Trends Neurosci.* **25**, 558 (2002).
- [6] M. N. Shadlen and W. T. Newsome, *J. Neurosci.* **18**, 3870 (1998).
- [7] P. H. E. Tiesinga, J. V. Josè, and T. J. Sejnowski, *Phys. Rev. E* **62**, 8413 (2000).
- [8] B. Agüera y Arcas, A. L. Fairhall, and W. Bialek, *Neural Comput.* **15**, 1715 (2003).
- [9] D. Brown, J. Feng, and S. Feerick, *Phys. Rev. Lett.* **82**, 4731 (1999).
- [10] H. Hasegawa, *Phys. Rev. E* **61**, 718 (2000).
- [11] L. Gammaitoni, P. Hänggi, P. Jung, and F. Marchesoni, *Rev. Mod. Phys.* **70**, 223 (1998).
- [12] H. Gang, T. Ditzinger, C. Z. Ning, and H. Haken, *Phys. Rev. Lett.* **71**, 807 (1993).
- [13] A. S. Pikovsky and J. Kurths, *Phys. Rev. Lett.* **78**, 775 (1997).
- [14] B. Lindner, J. García Ojalvo, A. Neiman, and L. Schimansky-Geier, *Phys. Rep.* **392**, 321 (2004).
- [15] E. Manjarrez, J. G. Rojas-Piloni, I. Méndez, L. Martínez, D. Vélez, D. Vázquez, and A. Flores, *Neurosci. Lett.* **326**, 93 (2003).
- [16] K. Pakdaman, S. Tanabe, and T. Shimokawa, *Neural Networks* **14**, 895 (2001).
- [17] B. Lindner, L. Schimansky-Geier, and A. Longtin, *Phys. Rev. E* **66**, 031916 (2002).
- [18] A. Longtin, *Phys. Rev. E* **55**, 868 (1997).
- [19] P. L. Gong, J. X. Xu, and S. J. Hu, *Chaos, Solitons Fractals* **13**, 885 (2002).
- [20] S. G. Lee, A. Neiman, and S. Kim, *Phys. Rev. E* **57**, 3292 (1998).
- [21] Y. Yu, W. Wang, J. Wang, and F. Liu, *Phys. Rev. E* **63**, 021907 (2001).
- [22] A. Neiman, B. Shulgin, V. Anishchenko, W. Ebeling, L. Schimansky-Geier, and J. Freund, *Phys. Rev. Lett.* **76**, 4299 (1996).
- [23] D. Noble and R. B. Stein, *J. Physiol. (London)* **187**, 129 (1966).
- [24] J. Rinzel and R. Miller, *Math. Biosci.* **49**, 27 (1980).
- [25] F. Rieke, D. Warland, R. de Ruyter van Steveninck, and W. Bialek, *Spikes: Exploring the Neural Code* (Massachusetts Institute of Technology: Cambridge, Massachusetts, 1996).
- [26] C. E. Shannon, *Bell Syst. Tech. J.* **27**, 379 (1948); *ibid.* **27**, 623 (1948).
- [27] T. M. Cover and J. A. Thomas, *Elements of Information Theory* (John Wiley and Sons, New York, 1991).
- [28] J. D. Farmer, *Z. Naturforsch. A* **37A**, 1304 (1982).
- [29] P. Grassberger, e-print physics/0307138.
- [30] R. S. Chikara and J. L. Folks, *The Inverse Gaussian Distribution* (Marcel Dekker, New York, 1988).
- [31] W. J. Wilbur and J. Rinzel, *J. Theor. Biol.* **105**, 345 (1983).
- [32] H. A. Kramers, *Physica (Amsterdam)* **7**, 284 (1940).
- [33] G. J. Escalera Santos, M. Rivera, and P. Parmananda, *Phys. Rev. Lett.* **92**, 230601 (2004).
- [34] *The Synaptic Organization of the Brain*, edited by G. M. Shepherd (Oxford University Press, New York, 2004).
- [35] F. Liu, J. Feng, and W. Wang, *Europhys. Lett.* **64**, 131 (2003).
- [36] E. Salinas and T. J. Sejnowski, *Nat. Rev. Neurosci.* **2**, 539 (2001).
- [37] I. M. Raman and L. O. Trussell, *Neuron* **9**, 173 (1992).